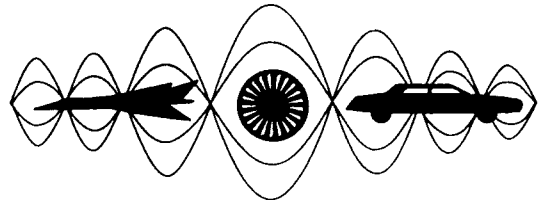

FIFTH INTERNATIONAL CONGRESS ON SOUND AND VIBRATION
DECEMBER 15-18, 1997
ADELAIDE, SOUTH AUSTRALIA

POWER FLOW USING ELECTRO - OPTIC HOLOGRAPHY, PART 1: OBTAINING THE STRUCTURAL PHASE

Gary A. Fleming* and Dr. Jonathan D. Blotter**

*National Aeronautics and Space Administration - Langley Research Center
Hampton, Virginia, USA

**Idaho State University, College of Engineering
Pocatello, Idaho, USA

ABSTRACT

Electro-Optic Holography (EOH) is a laser based, full field diagnostic technique used to measure micron sized deflections in statically displaced or vibrating structures. When applied to dynamically excited objects, EOH yields the time averaged displacement profile of the object surface. To obtain the structural power flow from EOH measurements, the structural phase must be extracted. This paper provides an overview of the EOH technique and describes a novel method successfully used to obtain the vibrational phase from EOH measurements. Experimental results from a sinusoidally driven cantilever beam are presented in support of this new method.

1.0 INTRODUCTION

Electro-Optic Holography (EOH) has been under development as a full-field, non-contacting measurement technique for measuring displacement fields of statically and dynamically excited objects since the 1970's. In contrast to scanning vibrometry, which performs point-wise scans of the object to obtain the dynamic velocity field, EOH measures the time averaged displacement profile of the entire surface, at video rates.

EOH and related techniques such as Electronic Speckle Pattern Interferometry (ESPI) [1] and phase-step interferometry [2] use single frequency lasers and CCD cameras to electronically record holograms of an object under various states of stress. For static deformations,

differencing two holograms of the same object under different loads produces holographic fringes indicative of the relative object displacement. In general, each fringe represents one additional laser wavelength of displacement. Lasers employed in most systems operate between 0.5 and 1.0 μm. Advanced image processing can extend this resolution to, conservatively, 1/20→1/50 of a fringe, producing deformation resolutions on the order of 25 nanometers. Being video based, the entire deformation field is measured simultaneously, at near video rates (30 Hz), with high spatial densities. Imaging a 0.5-x 0.5-meter test specimen with a generic 640-x 480-pixel camera yields sub-millimeter spatial resolutions, with no discontinuities between measurement sites. Figure 1 compares scanning vibrometry and EOH results of a dynamically forced aircraft fuselage panel along with FEM predictions [3]. The difference in spatial resolution is apparent.

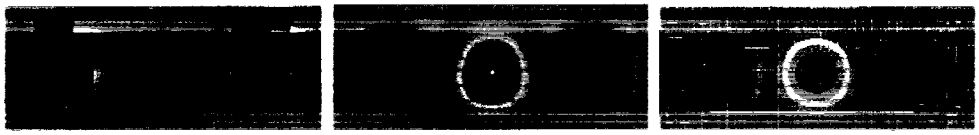

(a) (b) (c)

Figure 1: (a) Scanning vibrometry and (b) EOH measurements of aircraft fuselage panel mode shape, (c) FEM prediction. Region of interest: 18.5-x 47.5-mm.

When applied to vibrating objects, traditional EOH yields the time averaged displacement profile of the object surface. Since CCD cameras are time integrating devices, the displacement vs. time history is lost. For many applications, such as operating mode shape characterization, this information is not required. However, to determine higher order structural properties, the amplitude ***and*** phase of the complex valued velocity field must be known. The flow of energy or power through a structure is one such example. Measurement of structural power flow using holographic techniques has been addressed previously in the literature [4]. In this case, photographic holography was used with a double-pulsed, double reference beam configuration to preserve the high frequency, time dependent motion of the structure. The goal of the current investigation is to obtain power flow measurements using conventional EOH methods. As a first step, a method used to extract the vibrational phase will be described and applied to a sinusoidally excited cantilever beam.

2.0 EOH FUNDAMENTALS

The physics of EOH for statically and dynamically deformed objects has been treated extensively in the literature [5-9]. Example holographic fringe patterns of an object under static and dynamic loading are shown in Fig. 2. To understand how fringes are generated and the differences between statically and dynamically generated fringes, the following discussion is provided.

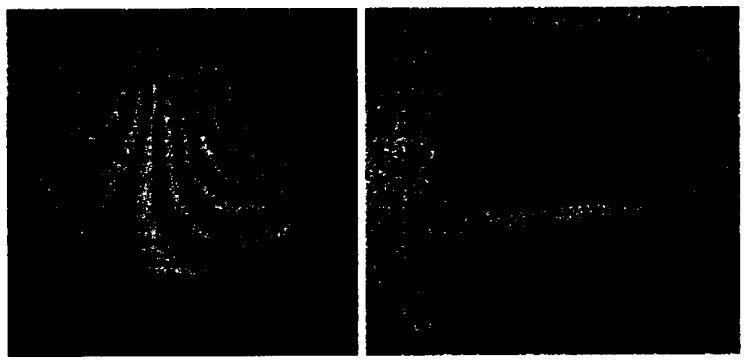

(a) (b)

Figure 2: Fringe patterns of a 23-x 23-cm aluminum plate under (a) static and (b) dynamic loading

EOH relies on specular interference of coherent light to obtain optical phase differences between the interfering waves in terms of intensity, which can be recorded by the CCD camera. Figure 3 presents a typical EOH setup, where a single laser beam is split to construct an *illumination leg* and *reference leg*. To obtain optimal interference, the path lengths of each leg are matched well within the coherence length of the laser. Diffusely scattered light from the test object is collected by the lens, and combined with the reference light at the beam splitter. The resulting hologram imaged on the CCD is electronically recorded.

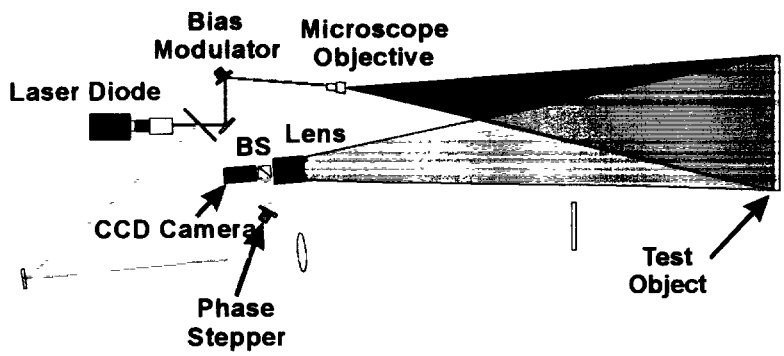

Figure 3: Typical EOH configuration

Assuming a stationary test specimen, the intensity of the hologram I_H at any point (x,y) on the CCD array can be described as:

$$I_H(x,y) = I_O(x,y) + I_R(x,y) + 2\sqrt{I_O I_R}\cos[\phi_O(x,y) - \phi_R(x,y)] \qquad (1)$$

where I_O is the intensity of the light scattered by the object, I_R is the intensity of the reference light, and ϕ_O, ϕ_R are the object and reference light phases, respectively. Now assume the test object has been statically deformed such that at least 1 point (x', y') has deformed an integer number of laser wavelengths $n\lambda$ from its reference condition. The displacement induced phase change of the object light is $nk\lambda$, where k is the wave number $(2\pi/\lambda)$. Thus, the intensity of the deformed object hologram I_H' is:

$$I_H'(x',y') = I_O'(x',y') + I_R(x',y') + 2\sqrt{I_O I_R}\cos[\phi_O(x',y') - \phi_R(x',y') + 2\pi n] \quad (2)$$

For small displacements, I_O remains constant. Therefore, for those regions of the object that have undergone displacements of $n\lambda$, $I_H' = I_H$. Thus, if holograms of an object are electronically recorded under two states of stress and differenced, the resulting image will contain black bands, or holographic fringes, whose fringe order n corresponds with n laser wavelengths of displacement. As inferred from equation (2), areas between the fringes will vary cosinusoidally in intensity.

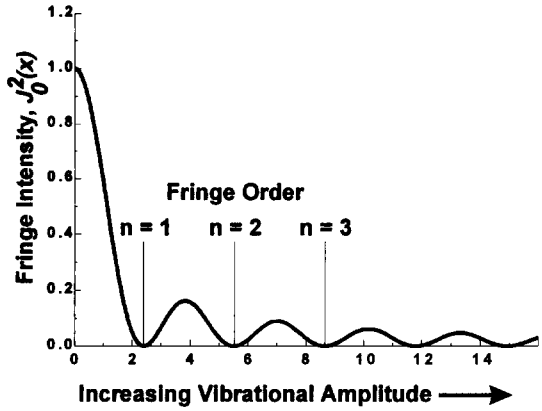

Figure 4: Fringe intensity distribution of dynamically loaded structures

Holographic fringes generated by vibrating objects are characteristically different than the static deformation case. Consider a cosinusoidally varying load applied to the test specimen. The displacement induced phase of the object beam can be described by:

$$\phi_V(x,y,t) = kL(x,y,t)) \quad (3)$$

where the subscript V denotes the *vibrating* object, and $L(x,y,t) = A_L(x,y)\cos(\omega t + \phi_L(x,y))$ is the oscillatory load with amplitude A_L, circular frequency ω, and structural phase ϕ_L. Thus, the intensity of the hologram will be time dependent, modulated by the excitation. Dropping the notation (x,y) for clarity:

$$I_V(t) = I_0 + I_R + 2\sqrt{I_0 I_R}\cos[\phi_0 - \phi_R + \phi_V(t)] \quad (4)$$

Assuming the period of excitation is much shorter than the integration time of the CCD, the recorded intensity is the time average of equation (4) over the camera's exposure. Upon rigorous derivation and virtual reconstruction of the hologram with a reference wave, it can be shown that the reconstructed holographic fringe intensity $I_{V,Rec}$ is proportional to the zero order Bessel function of the first kind squared [6]:

$$I_{V,\mathrm{Rec}} \propto J_0^2(\Omega(t)) \quad (5)$$

The function $\Omega(t)$ is the fringe-locus function, representing temporal phase changes of the object-scattered light. The relation in Eq. (5) is plotted in Fig. 4. In the reconstructed hologram, dark fringes will form when the fringe-locus function evaluates to a root of J_0^2. These fringes are directly related to the amplitude $A_L(x,y)$ of the surface oscillation. For symmetric illumination and observation vectors, the separation distance between fringes is approximately equal the laser wavelength λ. Nodal positions on the object can be clearly identified, since those regions with zero displacement appear approximately 6 times brighter than the rest of the image. For example, the zero-order fringe is readily identified in Fig. 2.

3.0 QUANTITATIVE DISPLACEMENT ANALYSYS

The process of obtaining quantitative displacements from electronically recorded holograms is depicted in Fig. 5. A 380-x 50-x 1.2-mm aluminum cantilever beam was used as the test specimen. The beam was driven with a piezoelectric actuator mounted near the free end. Results from a 50-x 225-mm region of the beam excited at 304 Hz are shown in Fig. 5, beginning with the raw fringe image, Fig. 5a. To obtain quantitative displacements, the displacement induced phase shift $\phi_D(x,y)$ must be determined for each imaged point (x,y) on the object surface. The total phase difference between the object-scattered and reference light is the summation of ϕ_D and a spatially random component, $\phi_O(x,y) - \phi_R(x,y)$. Several methods to eliminate the random phase have been devised, all which require the recording of a series of holograms with a known optical phase step between each CCD exposure. The phase step is typically generated by a piezoelectrically driven mirror placed in the reference leg of the EOH system, Fig. 3. The device is commonly known as a phase stepper. Three step [10], four step [11-12], and five step [13] approaches have been developed. For dynamically loaded objects, a second phase stepper is placed in the illumination leg and oscillated at the object excitation frequency. This phase stepper is often called the bias modulator to avoid confusion with the reference leg phase stepper. The bias modulation is used to eliminate unknowns in the evaluation of $J_0^2(\Omega(t))$ to obtain the fringe-locus function. The procedure is described in [6].

Determination of the optical phase yields a wrapped phase map modulo 2π as shown in Fig. 5b. Generally, the wrapped phase map contains high spatial frequency noise. Limitations in most phase unwrapping algorithms require the removal of this noise. One of the most popular filtering routines is based on a spatial carrier/FFT technique, and is described in [14]. This method removes the high frequency spatial fluctuations, while maintaining the high contrast, high frequency 2π jumps between fringes needed by phase unwrapping algorithms. Figure 5c shows the wrapped phase map after filtering with the spatial carrier/FFT technique. Next, phase unwrapping and division by the wave number k yields the displacement profile, Fig. 5d. One should note the measured deformations are directionally sensitive. The measured component of deflection is defined by the bisector between the illumination and observation vectors, and is referred to as the *sensitivity vector.*

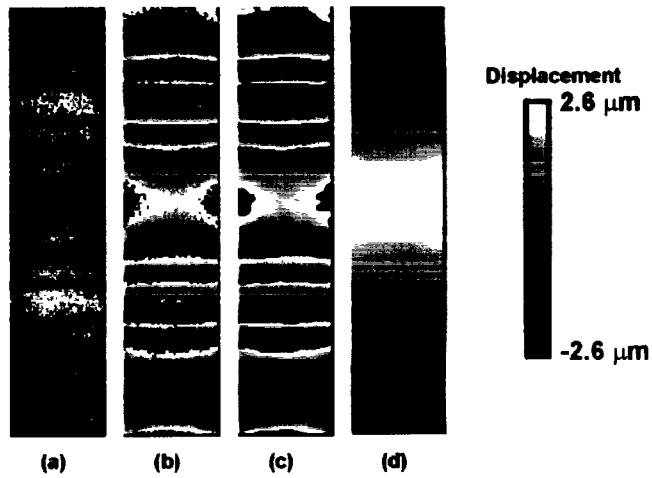

Figure 5: Stages to EOH processing: (a) raw fringes, (b) wrapped phase map, (c) filtered wrapped phase map, (d) displacement profile

4.0 OBTAINING THE STRUCTURAL PHASE

While conventional EOH can readily provide the time-averaged displacement amplitude of a vibrating object, it does not provide the complex-valued velocity field required for many structural mechanics problems. As a first step to obtain the time dependent velocity, a technique to measure the structural phase ϕ_L has been developed. Currently, EOH can determine the structural phase of objects at resonant modes, where portions of the object are either in or out of phase. This does not account for large structures whose parts may not be operating in a single mode or in conditions where the relative phase is not exactly 180°. Several other techniques to measure the structural phase have been described [1][15], but are not applicable to automated processing. In the present technique, the bias modulator frequency is adjusted to be slightly different than the object excitation to interject a low amplitude, low frequency beat. This frequency imbalance causes the holographic fringes to *sway* at the beat frequency, thus modulating the pixel intensities concomitantly. If a series of fringe maps is recorded at discrete time intervals, the intensity time history for each pixel can be reconstructed, and the phase can be determined using a Fourier transform algorithm.

The EOH system depicted in Fig. 2 was used to test the new technique. A single frequency, 200 mW laser diode lasing at 852 nm was used as the illumination source. The cantilever beam discussed in Section 3.0 was the test specimen. The forcing frequency of 304 Hz corresponds to a near resonance bending mode. The bias modulator was used to interject a beat frequency of 0.1 Hz, and a series of 64 images was acquired at 1 Hz. A portion of the time series is shown in Fig. 6. The shift in fringe position and periodic nature is quite apparent. The pixel intensity time history for two pixels located in antinodal regions is shown in Fig. 7. The data exhibits the expected 180° phase difference.

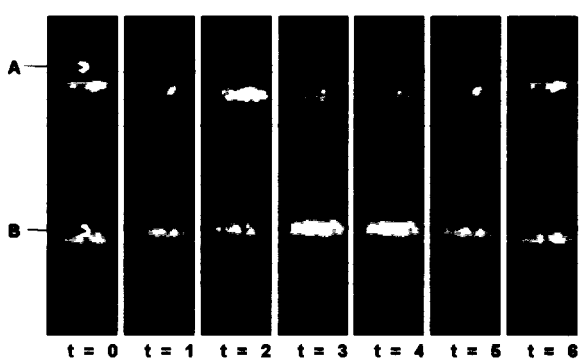

Figure 6: Fringe map time series with imposed beat frequency

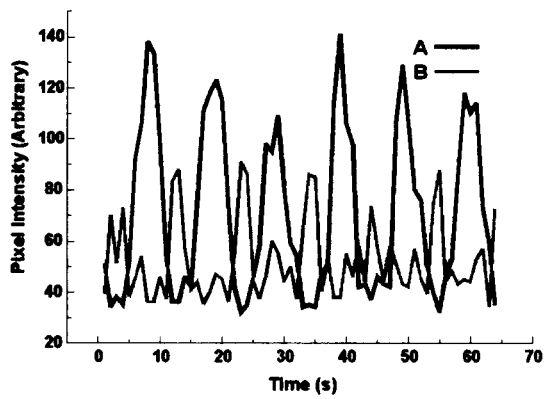

Figure 7: Intensity time series of pixels A and B marked in Fig. 6

After spatial filtering to remove speckle noise, the time domain FFT was computed for each pixel in the region of interest. The vibrational phase was then calculated from the real and imaginary transform coefficients at the beat frequency. Figure 8a again shows the raw fringe map, and the resulting phase map is shown in Fig. 8b. The calculated phase is modulo π since pixels on the opposing side of a fringe will be 180° out of phase. Phase unwrapping with the assistance of the displacement field shown in Fig. 5d produced the surface phase distribution, Fig. 8c. The mean relative phase was measured to be 180 ± 5.6°, the expected value for a beam oscillating in an operating mode. Pixels constituting the center column in

Fig. 8c have been plotted in Fig. 8d to show the phase distribution profile. It is important to note that exact resonance conditions were not obtained, and phase differences of several degrees resulting from structural damping are expected.

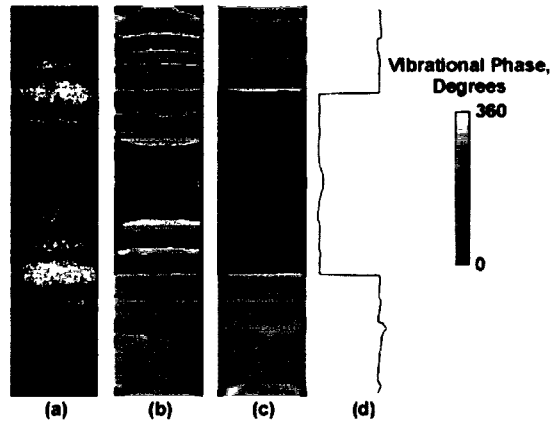

Figure 8: (a) Raw fringe map, (b) wrapped structural phase, (c) unwrapped structural phase distribution, (d) vertical profile

5.0 APPLICATION TO POWER FLOW

There are two basic methods which can be used to compute the power flow from these results. The first is based on a wave decomposition technique which lends itself to this method because the wave number has already been computed [4]. The second method consists of computing the power flow from the dot product of the generalized forces and velocities [16]. The generalized forces are computed from spatial derivatives of the displacement field.

Part 2 of this research will present and discuss the power flow results obtained from this newly developed technique. The results will be compared with analytical models as well as other experimental techniques.

6.0 CONCLUSIONS

The goal of this research effort was to develop a non-intrusive, whole-field measurement technique to extract power flow maps from vibrating structures. In this paper, a novel technique for extracting a complex representation of the velocity field, which provides the fundamental component for extracting the power flow, was developed. Although still in its infancy, this technique has been successfully used to measure the displacement field and the relative structural phase of a dynamically excited cantilever beam. Further research will statistically quantify the accuracy and reliability of this procedure as well as compute and present power flow results.

7.0 REFERENCES

1. Lokberg, O.J., and Slettemoen, G.A., "Basic Electronic Speckle Pattern Interferometry", in *Applied Optics and Optical Engineering*, Vol. X, 1987. Shannon, R.R., and Wyant, J.C. editors, pp. 455-504.
2. Creath, K., "Phase-measurement Interferometry: Beware These Errors", Proc. SPIE, **1553,** 213-220 (1991).
3. EOH and FEM analyses performed at NASA - Langley Research Center, Hampton, VA., December, 1996. Vibrometry results obtained by the Naval Research Laboratory, Washington, D.C., April, 1997.
4. Pascal, J.C., Carniel, X., Chalvidan, V., and Smigielski, P., "Determination of Structural Intensity and Mechanical Excitation using Holographic Interferometry," Proc.of the Structural Intensity and Vibration Energy Flow; 4th International Congress on Intensity Techniques, Senlis, France, pp. 137-144, (1993).
5. Jones, R. and Wykes, C., Holographic and Speckle Interferometry. Cambridge University Press, 1989.
6. Pryputniewicz, R.J., and Stetson, K.A., "Measurement of Vibration Patterns using Electro-Optic Holography", Proc. SPIE **1162,** 456-467 (1989).
7. Pryputniewicz, R.J., course notes from "Holographic Numerical Analysis", CHSLT - Worcester Polytechnic Institute. January, 1992.
8. George, N., "Speckle", Proc. SPIE **243,** 124-140 (1980).
9. Stetson, K.A., "Effects of Beam Modulation on Fringe Loci and Localization in Time-Average Hologram Interferometry", J. Opt. Soc. Am. **60,** 1378 (1970).
10. Wyant, J.C., Koliopoulos, C.L., Bhushan, B., and George, O.E., "An optical profilometer for surface characterization of magnetic media," ASLE Trans. **27**, 101-113 (1984).
11. Carré, P., "Installation et utilization du comparateur photoelectrique et interferentiel du Bureau International del Poids et Mesures," Metrologia **2**(1), 13-23 (1966).
12. Wyant, J.C., "Interferometric optical metrology: basic systems and principles," Laser Focus, 65-71 (May, 1982).
13. Hariharan, P., Oreb, B.F., and Eiju, T., "Digital phase-shifting interferometry: a simple error-compensating phase calculation algorithm," Appl. Opt. **26**(3), 2504-2505 (1987).
14. Takeda, M., Ina, H., and Kobayashi, S., "Fourier-transform method of fringe-pattern analysis for computer-based topography and interferometry," J. Opt. Soc. Am., **60**(1), 156-160 (1972).
15. Atcha, H., and Tatam, R.P., "Heterodyning of fibre optic electronic speckle pattern interferometers using laser diode wavelength modulation," Meas. Sci. Technol. **5**, 704-709 (1994).
16. Pavic, G., "Measurement of Structure Borne Wave Intensity, Part 1: Formulation of the Methods," J. Sound and Vibration, **49**(2) pp. 221-230, (1976).